Astragalus polysaccharide alleviates transport stress-induced heart injury in newly hatched chicks via ERS-UPR-autophagy dependent pathway

Jian Chen,* Yi-Xi Tang,* Jian-Xun Kang,* Ya-Ru Xu,* Ahmed Ibrahim Ahmed Elsherbeni,[†] Hassan Bayoumi Ali Gharib,[‡] and Jin-Long Li ⑩*,§,#,[1]

*College of Veterinary Medicine, Northeast Agricultural University, Harbin 150030, PR China; [†]Animal Production Research Institute, Agricultural Research Centre, Giza, Egypt; [‡]Animal Production Department, Faculty of Agriculture, Cairo University, Cairo, Egypt; [§]Key Laboratory of the Provincial Education, Department of Heilongjiang for Common Animal Disease Prevention and Treatment, Northeast Agricultural University, Harbin 150030, PR China; and [#]Heilongjiang Key Laboratory for Laboratory Animals and Comparative Medicine, Northeast Agricultural University, Harbin 150030, PR China

ABSTRACT Transport stress (**TS**) not only affects animal welfare but also eventually leads to higher morbidity and mortality. Moreover, TS could induce heart injury in animals, but the possible mechanism has yet to be fully explored. Astragalus polysaccharide (**APS**) is a main active component of *Radix Astragali*, which has an extensive anti-stress effect. However, the effect of APS on TS-induced heart injury has not yet been elucidated. In this study, a chick model of simulated TS was used. 240 newly hatched chicks were arranged into 4 groups: Control (**Con**), Transport group (**T**), Transport + water group (**TW**), and Transport + APS group (**TA**). Before transport, the chicks of the TW and TA groups were treated with deionized water and APS (0.25 mg/mL, 100 µL) by oral drops respectively. The histopathological analysis of myocardial tissue was assessed by hematoxylin and eosin staining. qRT-PCR and Western Blotting assays were employed to measure the expression of genes and proteins. Semiquantitative PCR was performed for the X box-binding protein-1 (**XBP-1**) mRNA splicing assay. The results indicated that APS significantly reduced TS-induced myocardial histopathological changes. Meanwhile, TS induced endoplasmic reticulum stress (**ERS**), evidenced by an activation of the unfolded protein response (**UPR**) signaling pathway and up-regulation of ERS-markers ($P <$ 0.05). Moreover, TS markedly triggered autophagy induction by activating AMP-activated protein kinase (**AMPK**), reflected by augmented LC3-II/LC3-I, AMPK phosphorylation and autophagy-related genes (**ATGs**) expression ($P <$ 0.05). Importantly, our study manifested that treatment of APS could reduce TS-induced ERS and AMPK-activated autophagy, accordingly alleviating heart injury of transported chicks. In summary, these findings indicate that TS induces heart injury in chicks via an ERS-UPR-autophagy-dependent pathway, and APS as an effective therapeutic method to alleviate it.

Keywords: transport stress, newly hatched chick, Astragalus polysaccharide, heart injury, endoplasmic reticulum stress

INTRODUCTION

Multiple evidences indicated that some stress, including heat stress (Yin et al., 2020), hypoxia (Park and Suzuki, 2007), shock, and panic (Pittig et al., 2013) could cause damage to the structure or function of the heart. It is well known that animal transport is usually accompanied with many detrimental stresses, including crowding, thermal microenvironment changes, oxygen-poor, body bumps, noise, environmental pollutants, and water or feed poor, which make transport stress (**TS**) high complicated (Broom, 2005). TS not only affects animal welfare (Santurtun and Phillips, 2015) but also eventually leads to higher morbidity and mortality (Machovcova et al., 2017). What is worse, according to a previous report, heart injury was found in animals after transport (Wan et al., 2016). Cardiomyocyte, as postmitotic cell, has almost no replication capability in maturity. In other words, due to the unsubstitutability of cardiomyocytes, heart injury is largely irreversible. However, how TS induced heart injury is not yet fully

illustrated. Moreover, little attention was paid to its alleviation. Accordingly, it is valuable to explore the mechanism of TS-induced heart injury and find a method to alleviate it.

Recently, a study has indicated that exogenous stress-induced heart injury might have been coupled with endoplasmic reticulum stress (**ERS**) and autophagy (Cui et al., 2022; Ge et al., 2022a). ERS is considered the primary and common cellular response to various stresses, which motivates the unfolded protein response (**UPR**) to degrade and clean proteins that misfolded or unfolded in the endoplasmic reticulum (**ER**) lumen. PKR-like ER kinase (**PERK**), inositol-requiring enzyme 1 (**IRE1**), and activating transcription factor 6 (**ATF6**) triggers the 3 main signaling pathways of UPR, respectively (Almanza et al., 2019; Ge et al., 2022a). In the normal physiological state, glucose regulated protein78kD (**GRP78**) binds to ATF6, IRE1 and PERK within the ER lumen. Once ERS occurs, GRP78 detaches from them and activates the ERS signal transduction pathway (Ge et al., 2022b; Pincus et al., 2010). Excessive ERS induced by external stress activates autophagy and apoptosis, subsequently causing cytotoxicity. Moreover, all 3 arms of UPR regulate autophagy (Cybulsky, 2017). The UPR is activated to clear misfolded proteins, either inducing their proper refolding or delivering them for degradation by autophagy (Zhu et al., 2022). Basic autophagy (usually at a low level) maintains intracellular balance by degrading organelles and lysosomal toxic proteins, but autophagy either could be fuelled by stress or induces programmed cell death. AMPK is a central regulator of autophagy, which can respond to various stresses (Lin et al., 2018). Activated-AMPK regulates autophagy-related genes (**ATGs**) transcription and promotes autophagy. The induction of ERS-UPR and autophagy play a key role in stress-induced heart injury (Vanhoutte et al., 2021). Although many experiments have conducted extensive investigations on TS, it is yet indistinct whether TS could induce heart injury by ERS-UPR-autophagy dependent pathway.

In recent years, traditional herbal medicine or its extract has been widely applied in the clinic as a supplemental or alternative medicine for the treatment or prevention of various diseases. Astragalus polysaccharide (**APS**), the principal active ingredient in the traditional herbal called *Radix Astragali*, has been proven to exert a variety of beneficial biological effects. Scientific studies demonstrated that APS could alleviate multiple stresses induced by exogenous poisons or adverse environment (Dai et al., 2021), such as heat stress (Ge et al., 2021b; Zeng et al., 2020), immune stress (Liu et al., 2015), oxidative stress (Jin et al., 2014, Ge et al., 2017), and inflammatory stress (Huang et al., 2022; Luo et al., 2015). Moreover, in western herbal therapy, APS was employed as a therapeutic medicine for the treatment of viral infections (Jiang et al., 2010, 2021), immune system disorders (Liu et al., 2015), and cancer (Zhou et al., 2018). Hence, APS exerts effective and extensive anti-stress effects, but the role of APS in TS-induced heart injury is still unclear.

In this study, we found that TS caused heart injury in newly hatched chicks. We further elucidated that APS alleviates TS-induced heart injury by reducing ERS and UPR, and suppressing AMPK-activated autophagy, suggesting a feasible therapy to antagonism heart injury induced by stress.

MATERIALS AND METHODS

Animal Ethics

All experimental methods and humane end points for decreasing pain in animals were performed according to institutional animal care and use committee (**IACUC**) guidelines under protocols approved by the Institutional Animal Care and Utilization Committee of Northeast Agricultural University (Harbin, China).

Animal Experiment and Treatment

In total, 240 chicks (female; newly hatched, Hy-Line Variety White) were gained from the Xianfeng Chicken Farm (Harbin, China) and assigned into 4 groups (n = 60): Control (**Con**), Transport group (**T**), Transport + deionized water group (TW), and Transport + APS group (**TA**). A chick model of simulated TS was developed based on previous studies (Dadgar et al., 2012; Ge et al., 2017; Li et al., 2021). Briefly, the Con group chicks were placed on a stationary electric cradle (0 cycle/min), but the chicks of T, TW, and TA groups were transported by a moving electric cradle (50 cycles/min, swinging back and forth) for 2, 4, and 8 h. All experimental animals stayed in a constant temperature and humidity environment (28°C and 50% relative humidity). Before simulation transport, the chicks of the TW and TA groups were, respectively, treated with deionized water and APS (0.25 mg/mL) by oral drops. The dose of APS was determined by the manufacturer's guidance and our pretest (Beijing Centre Biology Co., LTD, Beijing, China). All groups were prohibited from water and feed during the process of experiment. After TS treatment, the chicks were euthanized using carbon dioxide. The heart from each animal was rapidly collected on a cold plate and subsequently placed at −80°C for further research. Small pieces of heart tissue were collected and then fixed in 4% formaldehyde solution for histopathological observation.

Hematoxylin and Eosin (H&E) Staining

Heart tissues were dehydrated in ethanol, and paraffin embedded. A series of 5 μm microsections were stained with H&E to evaluate cardiomyocyte damage. The slices were scanned using a digital whole slide scanning system (Aperio AT2, Leica Biosystems, Nussloch, Germany). The heart damage score was scored according to a previously described (Yin et al., 2020, Zhao et al., 2021a, 2021b, 2021c). Briefly, 4 fields were randomly selected from the slices in different groups at different time points. The scoring rules are as follows: slight granule denaturation ($\rightarrow$, 1 point), vacuolar degeneration

(↑, 2 points), capillary congestion (Δ, 3 points), and necrosis (←, 4 points).

Quantitative Real-Time PCR

Total RNA was extracted from heart tissue (200 mg) using RNAout reagent (Beijing Tiandi, Inc., Beijing, China) following the manufacturer's description. The quality and concentration of the total RNA were determined spectrophotometrically at 260/280 nm. First-strand complementary DNA (**cDNA**) was produced from 2 μg total RNA using a commercial reagent kit (product category: AU311-02, TransGen Biotech, Beijing, China) following the manufacturer's description. The cDNA was stored at $-80°C$ before the quantitative Real-Time PCR (**qRT-PCR**) (Talukder et al., 2021; Zhao et al., 2022). The primers used in this study for qRT-PCR (**Table S1**, Supplementary material) were designed by the Primer Premier software 6.

Western Blot

Total protein was extracted from the heart tissue using RIPA Lysis buffer. Protein supernatant was separated by 10% SDS-PAGE and transferred onto a PVDF or NC membrane. The detail procedure of the Western blot is shown in Sun's report (Sun et al., 2018; Zhu et al., 2021). The membranes were washed 5 times for 5 min each, imaged by Amersham Imager 600 (GE, Boston, MA). Blots were semiquantified using Image J software (National Institute of Health, Bethesda, MD). Anti-ATF4 antibody (No. bs-1531R), anti-LC3 antibody (No. bs-8878R), anti-AMPK antibody (No. bs-4002R), anti-p-AMPK antibody (No. bs-5575R), and anti-GAPDH antibody (No. bs-2188R) were purchased from Bioss Biological Technology Co. Ltd. (Beijing, China). Anti-ATF6 antibody (No. A0202) and anti-Beclin1 antibody (No. A7353) were purchased from ABclonal Biological Technology Co. Ltd. (Wuhan, China).

X Box-binding Protein-1 (XBP-1) mRNA Splicing Assay

To assess the expression of XBP-1 (F: GGAGTGC-GAGTCTACGGATGT, R: CGGAGGTTGTCAG-GAATGGT), semiquantitative PCR was implemented using 2720 Thermal Cycler (Applied Biosystems, Shanghai, China). The methodological and quantitative details of this assay are as described in our previous study (Zhao et al., 2018, 2022). Briefly, the PCR product was run into 1.5% gel electrophoresis, and the GAPDH was used as the housekeeping reference gene. The gel was stained by ethidium bromide solution, and the spliced 103 bp XBP-1 and unspliced 143 bp bands (**XBP-1s/XBP-1u**) were imaged in a gel documentation system.

Statistical Analysis

All study data were analyzed with GraphPad Prism 8.0 (GraphPad Software, San Diego, CA) software. Statistical analysis was performed using one-way ANOVA followed by Tukey's post hoc pairwise comparison. The heat map for the different expression genes was drawn using TBtools software (V1.09854, designed by CJ, www.tbtools.com). Principal component analysis and correlation analysis were accomplished by SPSS 17.0 (SPSS, Inc., Chicago, IL).

RESULTS

Histopathological Analysis of Myocardial Tissue

To value the effects of APS on heart microstructure in transported-chicks, histopathological analysis was performed. As shown in Figure 1A, the Con group was no abnormal pathological structure at 2 and 4 h after transport. The cardiomyocytes were arranged neatly, the structure was complete, and the boundaries were obvious, but only slight granule denaturation was found at 8 h. When exerted with TS for 2 h, a remarkable granule denaturation appeared in the cytoplasm. Meanwhile, vacuolar degeneration and capillary congestion were occurred for TS lasting 4 h. At 8 h, significant vacuolar degeneration, capillary congestion and cell necrosis distinguished by deep staining of nucleus were found. Importantly, APS treatment overtly relieved myocardial cell injury induced by TS, where simply slight vacuolar degeneration at 8 h. Consistent with these results, the myocardial damage score (Figure 1B) was remarkably higher in the T and TW treatments than in the Con and TA groups for TS lasting 4 and 8 h ($P < 0.01$), meanwhile, there was no overt alternation between the Con and TA group ($P > 0.05$).

Transcript Levels of ERS-UPR-related Genes

To determine whether TS could induce heart ERS, and whether APS could antagonize TS-induced ERS, the mRNA levels of ERS-UPR related genes were detected (Figure 2). At 2 h, there was no marked change in the levels of GRP78 ($P > 0.05$, Figures 2A and 2G), ATF6 (Figures 2B and 2G), eukaryotic initiation factor 2 alpha (**eIF2α**, Figures 2D and 2G), and inositol-requiring enzyme 1 (**IRE1**, Figures 2F and 2G) among 4 groups. Compared to the Con group, ATF4 (Figures 2E and 2G), and PERK (Figures 2C and 2G) mRNA levels were remarkably increased in T, TW, and TA groups ($P < 0.01$). Meanwhile, both T and TW groups notably improved the mRNA expression of GRP78, PERK and ATF4 at 4 and 8 h ($P < 0.01$). In surprise, no significant difference was observed between the Con and TA groups ($P > 0.05$). Of note, there was an overt decrease of ATF6 ($P < 0.01$) and IRE1 ($P < 0.05$) mRNA expression for TS lasting 4 h, however, when the TS lasted for 8 h, the transcript levels of both genes were evidently boosted in T and TW groups compared to the Con and TA groups ($P < 0.01$). Likewise, the mRNA level of eIF2α in the T and TW groups was markedly upregulated at 8 h ($P <$
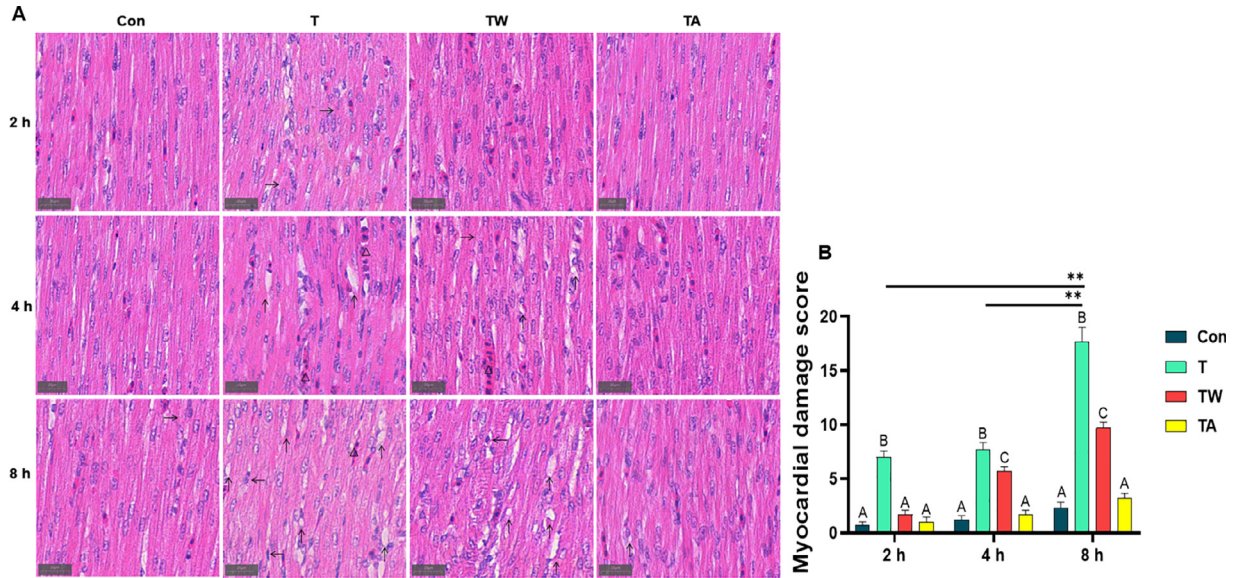
Figure 1. Effect of TS and APS on myocardial histopathological changes in transported-chicks. (A) Histopathology with hematoxylin and eosin staining of the heart section in different groups and different time points (Con, T, TW, and TA). (B) Myocardial damage score. Slight granule denaturation ($\rightarrow$, 1 point), vacuolar degeneration ($\uparrow$, 2 points), Capillary congestion (Δ, 3 points), necrosis ($\leftarrow$, 4 points). Data are presented as the mean $\pm$ SD. $*P < 0.05$ and $**P < 0.01$. At the same time point, the same letters mean the difference is not significant ($P > 0.05$), different small letters mean a significant difference ($P < 0.05$), and different capital letters for the extremely significant difference ($P < 0.01$).
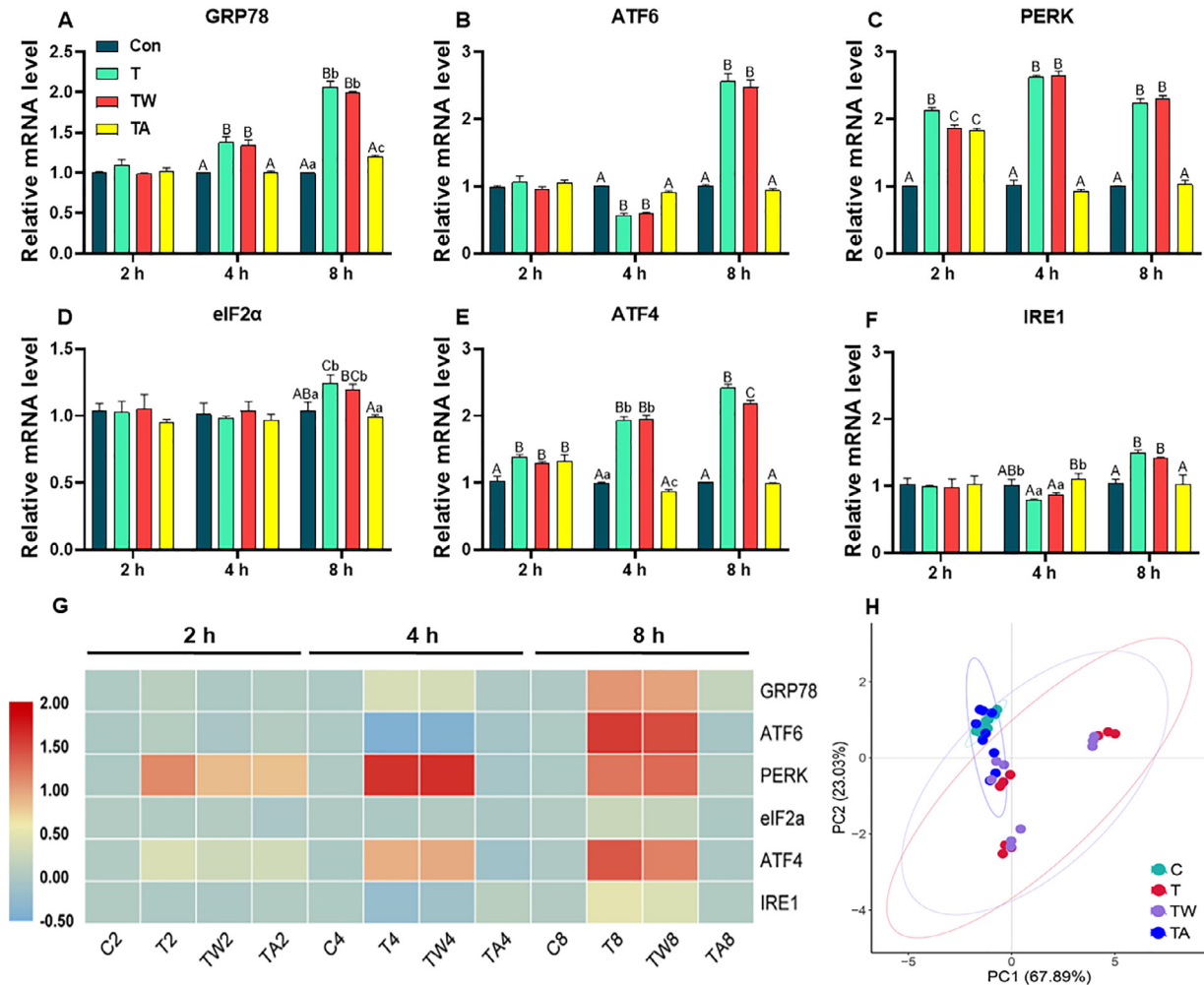
Figure 2. Effect of TS and APS on the transcript levels of ERS-UPR-related genes in transported-chicks. (A) GRP78, glucose regulated protein78kD. (B) ATF6, activating transcription factor 6. (C) PERK, protein kinase RNA-like ER kinase. (D) eIF2α, eukaryotic initiation factor 2. (E) ATF4, activating transcription factor 4. (F) IRE1, inositol-requiring enzyme 1α. (G) Heat map of relative mRNA levels of ERS-UPR-related genes. (H) PCA of ERS-UPR-related factor levels. Data are presented as the mean $\pm$ SD. $*P < 0.05$ and $**P < 0.01$. At the same time point, the same letters mean the difference is not significant ($P > 0.05$), different small letters mean a significant difference ($P < 0.05$) and different capital letters for the extremely significant difference ($P < 0.01$).

0.01 or $P < 0.05$), whereas no significant changes were recorded between the Con and TA group ($P > 0.05$).

PCA of Heart ERS-UPR Signaling Pathway

To determine the effects of TS and APS on the ERS-UPR, Principal Component Analysis (**PCA**) was implemented. The first and second principal components were 67.89 and 23.03%, respectively. Figure 2H showed that there is a large overlap between the T and TW group, indicating that providing water to the chicks before transport could not alleviate the TS-induced ERS. Importantly, the Con and TA groups almost completely overlap, suggesting that APS could effectively alleviate TS-induced ERS.

Protein Levels of ERS-UPR-related Factors

To further confirm APS could reduce the TS-induced heart ERS-UPR, we measured the protein levels of ERS markers ATF4 and ATF6. Consistent with the results of

mRNA expression, we observed significantly higher ATF4 protein expression in the group of T, TW and TA than in that of the Con group at 2 h ($P < 0.01$, Figures 3A and 3C). Surprisingly, the high expression of ATF4 induced by TS was normalized in TA group at 4 and 8 h. Concomitantly, the ATF6 protein level (Figures 3A and 3D) of all groups was no alternation at 2 h ($P > 0.05$), but at 4 h, T and TW groups significantly suppressed its expression ($P < 0.01$), and APS significantly reduced ($P < 0.05$) this inhibitory effect. On the contrary, the protein level, compared to the Con group, ATF6 level was elevated clearly in the T and TW groups at 8 h ($P < 0.01$), but obviously collapsed in the TA group ($P < 0.01$). Notably, at 4 h, the ATF6 level of T group was visibly lower than that at 2 and 8 h ($P < 0.01$).

XBP-1s/XBP-1u Ratio

The ratio of XBP-1s/XBP-1u is an ERS marker. Hence, we performed a mRNA splicing assay to analysis
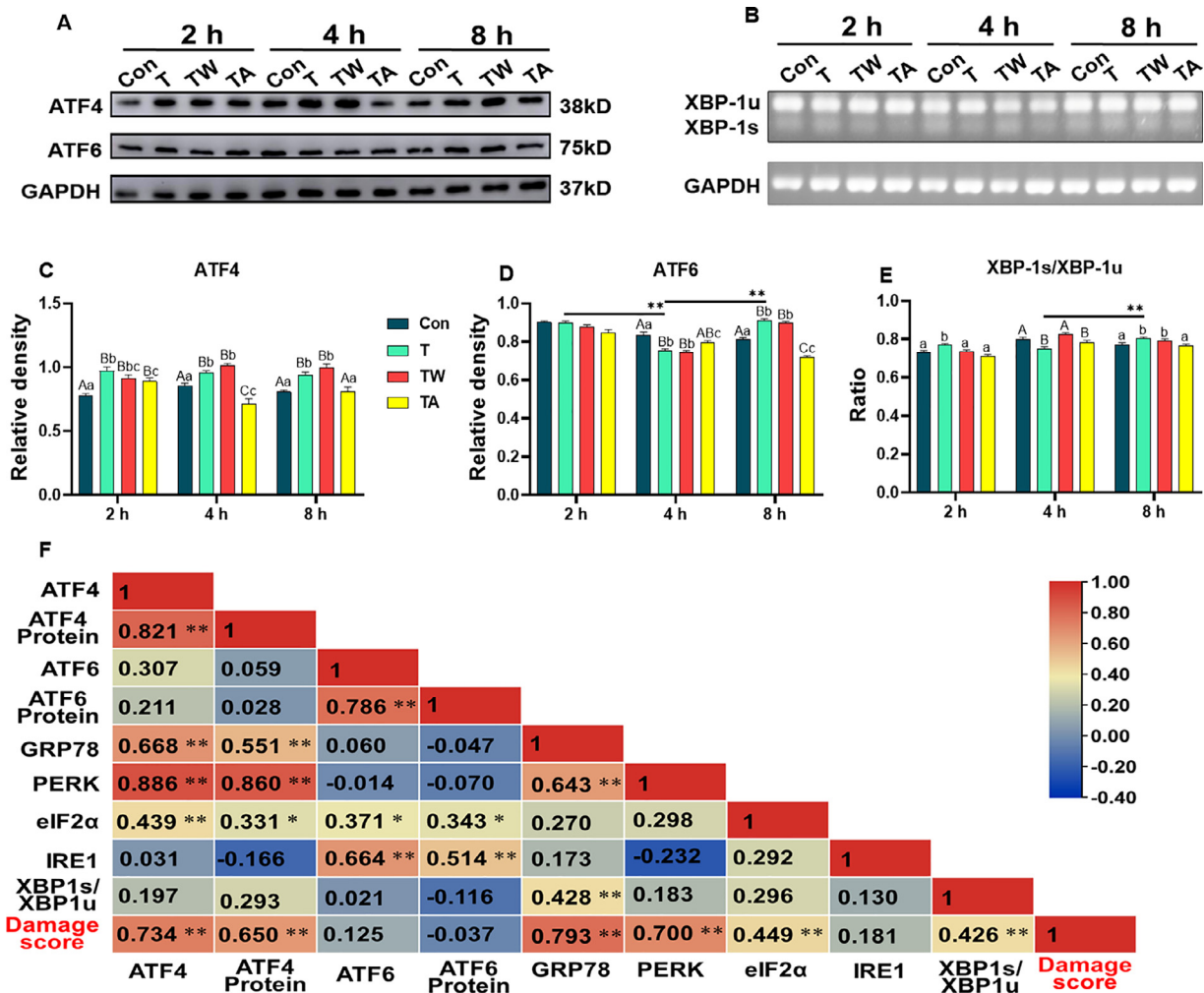
Figure 3. Effect of TS and APS on protein levels of ERS markers in transported-chicks. (A) The protein levels of ERS-UPR-related factors detected by Western blotting analysis; GAPDH was served as loading control for the total fractions respectively. (B) Luminance value analysis of XBP-1s/XBP-1u. (C) AFT4/GAPDH. (D) ATF6/GAPDH. (E) XBP-1s/XBP-1u. (F) Correlation analysis between ERS markers and damage score. Data are presented as the mean ± SD. *$P < 0.05$ and **$P < 0.01$. At the same time point, the same letters mean the difference is not significant ($P > 0.05$), different small letters mean a significant difference ($P < 0.05$) and different capital letters for the extremely significant difference ($P < 0.01$).

the nuclear factor XBP-1 mRNA splicing. As displayed in Figures 3B and 3E, XBP-1s/XBP-1u ratio in the T group at 2 h was remarkably elevated compared to the other groups ($P < 0.05$). Meanwhile, when TS lasted 4 h, XBP-1s/XBP-1u ratio was overtly reduced in the group of T and TA compared to the Con and TW group ($P < 0.01$). Furthermore, there was an apparent elevation of XBP-1s/XBP-1u ratio in the T and TW treatments for TS lasting 8 h in contrast to the Con group ($P < 0.05$), but this effect was normalized after APS treatment.

Correlation Analysis between ERS Markers and Damage Score

To further verify the connection between ERS and myocardial damage score, the correlation analysis was performed. As shown in Figure 3F, the damage score was notably positive correlated with the gene and protein expression levels of ATF4 ($P < 0.05$), and the mRNA levels of GRP78, PERK and eIF2α, together with the XBP-1s/XBP-1u ratio. Meanwhile, as expected, there is a remarkable ($P < 0.01$) positive correlation between the ATF4 and GRP78, PERK ($P < 0.01$) and eIF2α ($P < 0.05$) levels. Additionally, the mRNA and protein level of ATF6 was significantly positive correlated with the mRNA expression levels of eIF2α ($P < 0.05$) and IRE1 ($P < 0.01$). Furthermore, it was found that there was an evidently ($P < 0.05$) positive correlation between the XBP-1s/XBP-1u ratio and GRP78.

Gene Expression of AMPK and ATGs

To confirm the effects of TS and APS on heart autophagy, the mRNA levels of AMPKs (Prkaa1, a2, b1, b2, g2, and g3) and ATGs were analyzed in the present study. The mRNA levels of all AMPKs were no significant difference among all groups for TS lasting 2 h ($P > 0.05$, Figure 4A). However, compared to the Con group, the mRNA level of Prkaa2 and ag3 was evidently reduced in the T group at 4 h ($P < 0.05$), but all of which was normalized by APS treatment. When the TS subjected to chicks for 8 h, the a1 ($P < 0.05$), a2 ($P < 0.01$), and b1 ($P < 0.01$) relative mRNA levels of T and TW groups were overtly elevated, and the b2 level was reduced ($P < 0.05$) in contrast to the Con, importantly, all of these changes were restored in TA group.

The mRNA expression of Beclin1 (Figure 4B) and ATG5 (Figure 4F) were synchronous among each time point, showing that no remarkable difference was found among the 4 groups at 2 and 4 h, but displayed a notable elevation in the group of T and TW compared with the Con and TA treatment ($P < 0.01$). No marked difference ($P > 0.05$) was found in LC3 at 2, 4, and 8 h (Figure 4C), and mammalian target of rapamycin (**mTOR**, Figure 4D) at 2 h in all experimental groups compared to the Con group. Meanwhile, the mTOR expression was suppressed ($P < 0.01$) by TW treatment at 4 h, and

T treatment at 4 and 8h, but in the TA group, it was restored to normal (4 h) or higher level (8 h). Both P62 (Figure 4E) and ATG7 (Figure 4G) mRNA levels showed high expression after transport, which could be reverted by the APS. Furthermore, as presented in Figure 4I, compared to the Con and TA group, the mRNA levels of ATG16-2, ATG4b, ATG13, ATG2b, ATG9a, ATG9b and ATG14 in T and TW groups were significantly ($P < 0.05$ or $P < 0.01$) augmented at 4 and 8 h after TS. However, the levels of ATG3, ATG4a, ATG10 and ATG8 at 8 h, and ATG4c at 4 h and 8 h were remarkably decreased ($P < 0.05$ or $P < 0.01$). As shown in Figure 4J, the PCA analysis of autophagy-related factors showed that there was an apparent distance between the Con group and T or TW group. Additionally, the spacing between the Con and TA group was smaller than it between the Con group and the T or TW group.

Levels of Autophagy-related Proteins

To further confirm the APS could alleviate the AMPK-activated autophagy after subjected to TS, we analyzed the protein levels of autophagy signaling pathway in the chick heart. There was no apparent change in the level of AMPK total protein in all groups (Figures 5A and 5C; $P > 0.05$). However, a marked elevation ($P < 0.05$ or $P < 0.01$) was recorded of p-AMPK level (Figures 5B and C) in T group during the entire test period compared to the Con group. Meanwhile, the protein level of p-AMPK was augmented ($P < 0.01$) in the TW group at 2 and 4 h in contrast to the Con group. Importantly, in the TA group, the p-AMPK level was normalized after treated with APS at 4 h, and significantly decreased at 8 h compared to Con group ($P < 0.01$). Additionally, the level of Beclin1 (Figures 5C and E) was no apparent difference in the T and TW groups compared to the Con for the TS lasted 2 h ($P > 0.05$), but it was decreased significantly in the TA group ($P < 0.01$). Likewise, the Beclin1 protein expression of T group was markedly higher than that of Con and TA groups at 4 and 8 h ($P < 0.05$). Notably, the autophagy marker LC3II/I ratio (Figures 5D and 5F) in T group was significantly increased ($P < 0.05$ or $P < 0.01$) in a time-dependent manner. Moreover, the LC3II/I ratio was overtly increased in T and TW groups ($P < 0.01$), but it was normalized in TA group.

Correlation Analysis between Autophagy-related Factors and Damage Score

To further check the connection between autophagy-related factors and myocardial damage score, the correlation analysis was performed. As shown in Figure 5G, the damage score was notable positively correlated with the protein levels of p-AMPK ($P < 0.05$), Beclin1 ($P < 0.01$) and LC3II/I ($P < 0.05$), and the mRNA levels of
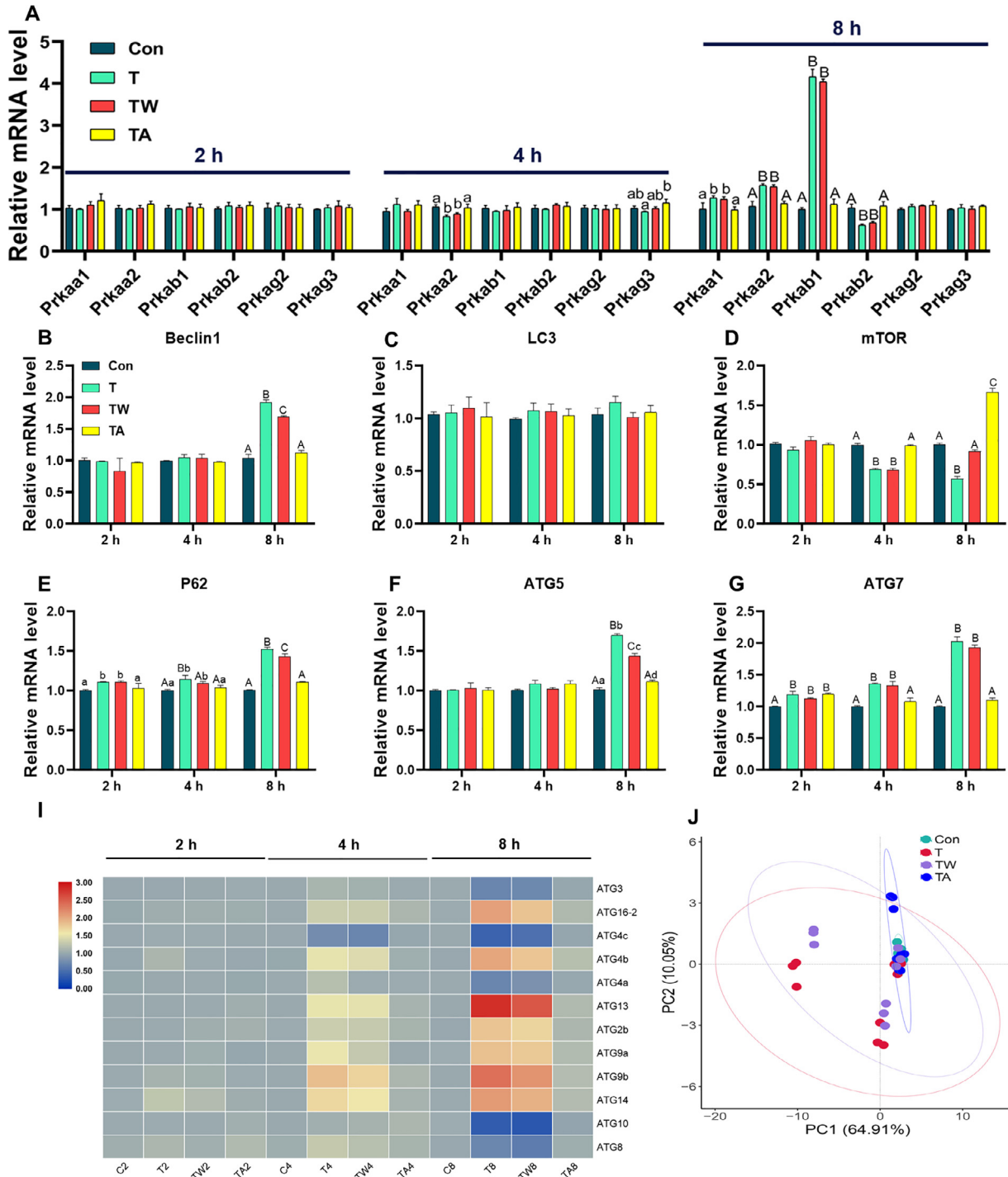
Figure 4. Effect of TS and APS on gene expression of AMPKs and ATGs in transported-chicks. (A) AMPK-associated subunits mRNA expression. (B) Beclin1. (C) LC3. (D) mTOR. (E) P62. (F) ATG7. (I) Heat map of relative mRNA levels ATGs. (J) PCA of the ERS-UPR-related factor levels. Data are presented as the mean ± SD. *$P < 0.05$ and **$P < 0.01$. At the same time point, the same letters mean the difference is not significant ($P > 0.05$), different small letters mean a significant difference ($P < 0.05$) and different capital letters for the extremely significant difference ($P < 0.01$).

Beclin1, P62, ATG5, and ATG7 ($P < 0.01$). Meanwhile, there was a marked negative correlation between the damage score and mTOR mRNA level ($P < 0.01$). Concomitantly, there was no overtly correlation ($P > 0.05$) between the AMPK protein and other factors. Of note, the mRNA and protein level of Beclin1 was marked positively ($P < 0.01$) correlated with the levels of ATG5, P62, and LC3II/I.

Correlation Analysis between ERS-UPR and Autophagy Signal Pathway

To estimate the crosstalk between ERS-UPR and autophagy signaling pathway, correlation analysis was performed for ERS markers and autophagy-related factors. As shown in Figure 6, there was a remarkably positive correlation between the ATF4 levels and ATG5
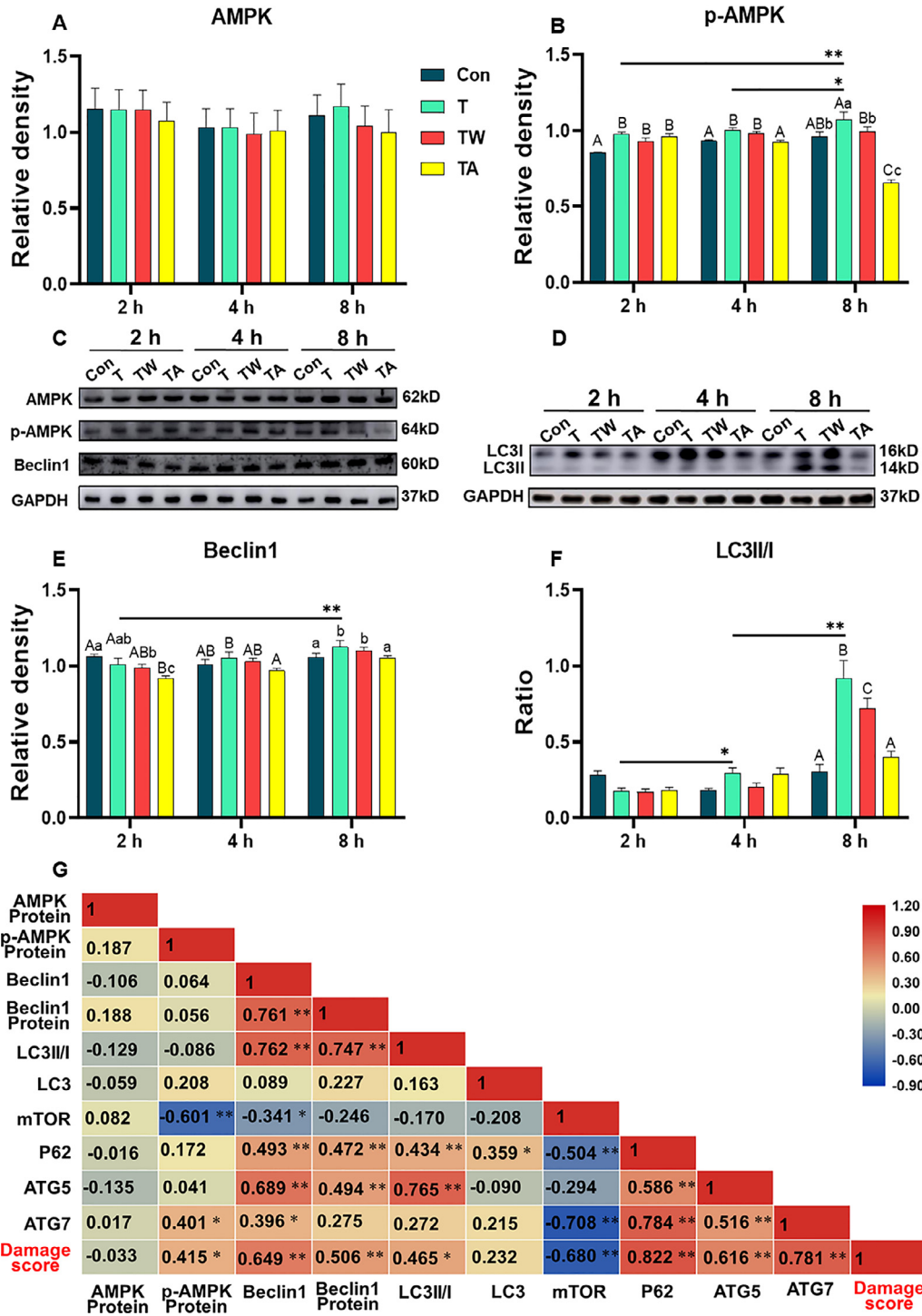
Figure 5. Effect of TS and APS on protein levels of autophagy signaling pathway in transported-chicks. (A) AMPK/GAPDH. (B) p-AMPK/GAPDH. (C, D) The protein levels of autophagy-related factors determined by Western blotting analysis; GAPDH was served as loading control for the total fractions respectively. (E) Beclin1/GAPDH. (F) LC3II/I ratio. (G) Correlation analysis between autophagy-related factors and damage score. Data are presented as the mean $\pm$ SD. *$P < 0.05$ and **$P < 0.01$. At the same time point, the same letters mean the difference is not significant ($P > 0.05$), different small letters mean a significant difference ($P < 0.05$) and different capital letters for the extremely significant difference ($P < 0.01$).

($P < 0.05$), P62 ($P < 0.01$), Beclin1 ($P < 0.05$), and p-AMPK levels ($P < 0.01$). However, it was found that there was a notably negative correlation between the XBP-1s/XBP-1u ratio and the Beclin1 levels ($P < 0.05$). Of note, an obvious ($P < 0.05$ or $P < 0.01$) positive or negative correlation were observed among ERS-UPR markers (GRP78 and eIF2α) and autophagy markers (LC3II/I, Beclin1, ATG5, P62, mTOR), suggested that

APS intervention may alleviate TS-induced heart injury via the crosstalk of ERS-UPR and autophagy.

DISCUSSION

The animals get panicked and restless as a result of the high temperature and shaking during transport, and
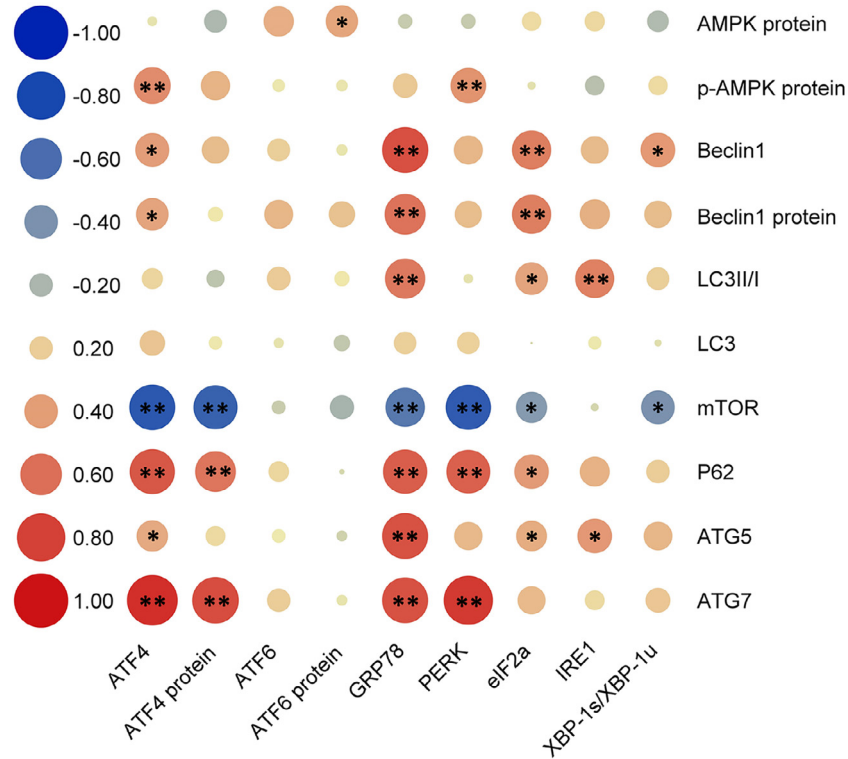
Figure 6. Correlation analysis between ERS-UPR and autophagy signal pathway.

they suffer scratches and bruises in the carriage, resulting in animal weight loss (Zhang et al., 2019), endocrine dysfunction (Ferlazzo et al., 2020), and poor immune function (Li et al., 2019). With high complexity, TS not only causes alternation in physiological metabolism, but may also induce organ damage (Wan et al., 2016). Moreover, our previous study demonstrated that TS induced heart damage and significantly decreased the weight of chicks (Li et al., 2017). It directly affects the production performance of animals and may eventually result in animal death (Machovcova et al., 2017). A previous study also indicated that TS induced heart injury in newly hatched chicks by increasing the production of nitric oxide and inhibiting the heat shock response (Sun et al., 2018), indicating that TS inhibited the cellular defense response, subsequently causing cell death and histopathological changes. The heart, as the central organ of the circulatory system, promotes blood flow, provides oxygen and various nutrients to the organs and tissues, and takes away the end products of metabolism, thereby keeping the cells normal metabolism. Animals often die suddenly during or after transportation, which may be related to heart failure induced by TS (Bao et al., 2008). An experiment on heart damage has shown that road transport could induce tissue and function damage to the heart reflected by an elevation of CK activity and histopathological damage of cardiomyocytes (Zhu et al., 2009). In the present study, we observed a significant histopathological change when TS lasted for 4 and 8 h, which demonstrated that TS could induce obvious heart injury. Importantly, these changes were restored by APS, indicating APS has the potential to alleviate TS-induced heart damage, and can be

employed as an effective strategy to resist TS in animal production.

ERS is a significant factor in many pathologies, including neurodegeneration, diabetes, and cancer (Oakes and Papa, 2015). Evidence from a previous report indicated that stress-activated ERS acts a vital role in tissue injury (Kim et al., 2013). Stress causes protein quality control system disorder in the ER lumen, which in turn induces ERS, and activates the cytoprotective UPR to induce a series of transcriptional and translational events that recover ER homeostasis. In addition, if ERS at high levels for a long time, a terminal UPR program will induce programmed cell death (Almanza et al., 2019). However, to the best of our knowledge, studies have not yet confirmed which ERS-UPR signaling pathways can be activated by TS and induce heart injury. The GRP78 is a trigger of the UPR due to its high affinity to misfolded proteins (Pincus et al., 2010). In this study, the mRNA level of GRP78 in T and TW groups was remarkably increased for TS lasting 4 and 8 h, which suggested that TS-induced ERS may increase in a time-dependent manner. ERS can be induced by 3 independent signaling pathways, including ATF6, IRE1, and PERK (Zhao et al., 2022). ATF-6 translocates to the Golgi apparatus, where it is cleaved and activated (Qin et al., 2021). The activated ATF-6 transfers to the nucleus and promotes ER associated degradation pathways (Li et al., 2021). Study manifested that heat stress induced cerebellar damage in mice via augmenting protein expression of ERS-related proteins (actived ATF-6 and PERK) (Oghbaei et al., 2021). Likewise, our results also indicated that TS significantly increased the activity of ERS-UPR signaling

pathways, including ATF6, PERK-eIF2α-ATF4, and IRE1-XBP1. It was reported that XBP-1s/XBP-1u is a marker of ERS degree (Zhao et al., 2018). When ERS occurs, XBP-1u is spliced to form XBP-1s, which up-regulates the expression of ER chaperones (Zhao et al., 2018). In this study, all ERS markers (GRP78, ATF6, PERK, eIF2α, ATF4, IRE1 and XBP-1s/XBP-1u) were significant elevated after subjected to TS for 4 or 8 h, but these alternations were regained by APS treatment. Furthermore, it was also supported by the PCA results, evidenced by a completely overlap between the Con and TA groups. Concomitantly, the correlation analysis showed that the damage score was significant positively correlated with the ERS markers. Evidently, the heart injury caused by TS was at least partly attributed to highly ERS induction, and APS alleviated its injury by reducing ERS.

Similarly, like UPR, autophagy is also one of the main responses of cell to stress (Qi and Chen, 2019). Autophagy induces cell death under excessive metabolic stress, and it may involve TS-induced cardiac damage (Dodson et al., 2013). As the common physiological adaptation of cells within the cell microenvironment, autophagy has a dual impact on cell regulation, either encouraging cell survival or accelerating cell death (Vanhoutte et al., 2021). Under severe stress conditions, autophagy could cause cell death (Barany et al., 2018; Vegliante and Ciriolo, 2018). As an energy sensor, AMPK has a close relationship with mTOR. Meanwhile, AMPK can reduce mTOR expression in multiple pathways, which exerts a vital role in autophagy induction (Barany et al., 2018). As a heterotrimer, AMPK is composed of α, β and γ subunits. Both the β subunit and the γ subunit are regulatory subunits, and the α subunit is the catalytic subunit. Phosphorylation of α subunit at threonine 172 residue is a key step in AMPK activated autophagy induction (Viollet et al., 2010). In the present study, TS down-regulated the mTOR level of chicks heart after 4h treatment and altered the AMPK associated subunits (a1, a2, b1, and b2) mRNA expression after 8h treatment. Moreover, there was no prominent difference in the total AMPK protein levels among each group, but the p-AMPK level
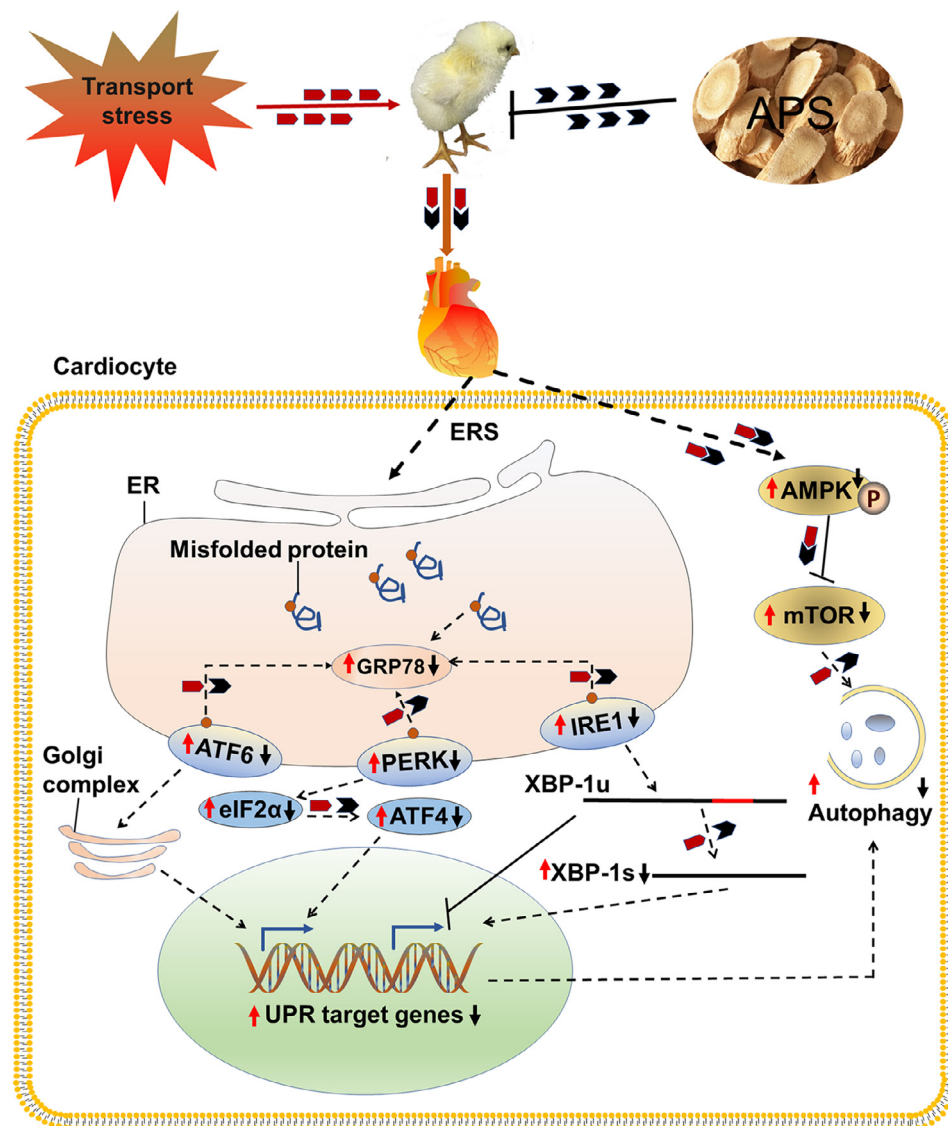
Figure 7. Schematic diagram illustrating the proposed mechanism of APS alleviates TS-induced heart injury mechanism in chicks via an ERS-UPR-autophagy dependent pathway.

and the autophagy marker LC3II/I ratio (after subjected to TS for 8h) were the highest in TS treatment. Importantly, compared to the TS treatment groups, the expression of these proteins recovered to a normal level in APS treatment. These results suggested that APS could moderate TS-induced cardiomyocyte autophagy by regulating AMPK signaling pathway.

On the other hand, the autophagy process is regulated by multiple evolutionarily conserved genes; these genes are named ATGs (Parzych and Klionsky, 2014). To further confirm whether TS could impact on the factors involved in autophagy flux, we analyzed the levels of mRNA or proteins relative to autophagy, such as Beclin1, Atg5, Atg7, Atg16-2 and other ATGs. Beclin-1, ATGs and p62 are involved in the initiation, elongation and degradation in the process of autophagy, respectively (Yin et al., 2021). The Atg12-Atg5-Atg16 complex is a crucial component in autophagosome formation, which is conducive to the expansion of phagosomes (Lystad et al., 2019). ATG7 activates LC3I, which is then conjugated to phosphatidylethanolamine by ATG3 to form LC3-II (Lystad et al., 2019). Previous investigation demonstrated that exogenous stress could lead to a prominent elevation of autophagy-related factors (Jamshed et al., 2019). In this study, the results revealed that elevated levels of Beclin1, P62, Atg5, Atg7, Atg16-2, ATG4b, ATG13, ATG2b, atg9a, ATG9b, and Atg14 after TS treatment. These results further revealed that TS could promote heart autophagy via regulating autophagy-related proteins. Importantly, those changes were mitigated by APS treatment, suggesting APS had an ameliorating effect on TS-induced heart autophagy. Besides, the PCA results of autophagy-related factors also supported it, reflected by a largely overlap between the Con and TA groups. Concomitantly, according to the results of correlation analysis between autophagy-related factors and damage score, the heart injury of transported-chicks may be related to AMPK-induced autophagy. Surprisingly, there was an obvious correlation between ERS-UPR markers and autophagy-related factors, which suggested that APS intervention may alleviate TS-induced heart injury via the crosstalk of ERS-UPR and autophagy signaling pathways.

CONCLUSIONS

To summarize, our study demonstrated, for the first time, that TS could cause ERS and induce autophagy, resulting in chicks' heart injury. Importantly, APS could alleviate TS-induced heart injury in chicks via an ERS-UPR-autophagy dependent pathway (Figure 7). Accordingly, the use of APS in newly hatched chicks before transport may be an effective strategy to alleviate TS-induced heart injury.

ACKNOWLEDGMENTS

DISCLOSURES

All authors declared that they have no relevant interest relationships.

SUPPLEMENTARY MATERIALS

Supplementary material associated with this article can be found in the online version at doi:10.1016/j.psj.2022.102030.

REFERENCES

Almanza, A., A. Carlesso, C. Chintha, S. Creedican, D. Doultsinos, B. Leuzzi, A. Luis, N. McCarthy, L. Montibeller, S. More, A. Papaioannou, F. Puschel, M. L. Sassano, J. Skoko, P. Agostinis, J. de Belleroche, L. A. Eriksson, S. Fulda, A. M. Gorman, S. Healy, A. Kozlov, C. Munoz-Pinedo, M. Rehm, E. Chevet, and A. Samali. 2019. Endoplasmic reticulum stress signalling - from basic mechanisms to clinical applications. FEBS J. 286:241–278.

Bao, E., K. R. Sultan, B. Nowak, and J. Hartung. 2008. Expression and distribution of heat shock proteins in the heart of transported pigs. Cell Stress Chaperones. 13:459–466.

Barany, I., E. Berenguer, M. T. Solis, Y. Perez-Perez, M. E. Santamaria, J. L. Crespo, M. C. Risueno, I. Diaz, and P. S. Testillano. 2018. Autophagy is activated and involved in cell death with participation of cathepsins during stress-induced microspore embryogenesis in barley. J. Exp. Bot. 69:1387–1402.

Broom, D. M. 2005. The effects of land transport on animal welfare. Rev. Sci. Tech. 24:683–691.

Cui, J. G., Y. Zhao, H. Zhang, X. N. Li, and J. L. Li. 2022. Lycopene regulates the mitochondrial unfolded protein response to prevent DEHP-induced cardiac mitochondrial damage in mice. Food Funct. 13:4527–4536.

Cybulsky, A. V. 2017. Endoplasmic reticulum stress, the unfolded protein response and autophagy in kidney diseases. Nat. Rev. Nephrol. 13:681–696.

Dadgar, S., T. G. Crowe, H. L. Classen, J. M. Watts, and P. J. Shand. 2012. Broiler chicken thigh and breast muscle responses to cold stress during simulated transport before slaughter. Poult. Sci. 91:1454–1464.

Dai, X. Y., Y. Zhao, J. Ge, S. Y. Zhu, M. Z. Li, M. Talukder, and J. L. Li. 2021. Lycopene attenuates di(2-ethylhexyl) phthalate-induced mitophagy in spleen by regulating the sirtuin3-mediated pathway. Food Funct. 12:4582–4590.

Dodson, M., V. Darley-Usmar, and J. Zhang. 2013. Cellular metabolic and autophagic pathways: traffic control by redox signaling. Free Radic. Biol. Med. 63:207–221.

Ferlazzo, A., E. Fazio, and P. Medica. 2020. Behavioral features and effects of transport procedures on endocrine variables of horses. J. Vet. Behav. 39:21–31.

Ge, J., K. Guo, Y. Huang, P. D. Morse, C. Zhang, M. W. Lv, and J. L. Li. 2022a. Comparison of antagonistic effects of nanoparticle-selenium, selenium-enriched yeast and sodium selenite against cadmium-induced cardiotoxicity via AHR/CAR/PXR/Nrf2 pathways activation. J. Nutr. Biochem. 21:108992.

Ge, J., K. Guo, C. Zhang, M. Talukder, M. W. Lv, J. Y. Li, and J. L. Li. 2021a. Comparison of nanoparticle-selenium, selenium-enriched yeast and sodium selenite on the alleviation of cadmium-induced inflammation via NF-kB/IkappaB pathway in heart. Sci. Total Environ. 773:145442.

Ge, J., Y. Q. Huang, M. V. Lv, C. Zhang, M. Talukder, J. Y. Li, and J. L. Li. 2022b. Cadmium induced Fak-mediated anoikis activation in kidney via nuclear receptors (AHR/CAR/PXR)-mediated xenobiotic detoxification pathway. J. Inorg. Biochem. 227:111682.

Ge, J., H. Li, F. Sun, X. N. Li, J. Lin, J. Xia, C. Zhang, and J. L. Li. 2017. Transport stress-induced cerebrum oxidative stress is not mitigated by activating the Nrf2 antioxidant defense response in newly hatched chicks. J. Anim. Sci. 95:2871–2878.

Ge, J., L. L. Liu, Z. G. Cui, M. Talukder, M. W. Lv, J. Y. Li, and J. L. Li. 2021b. Comparative study on protective effect of different selenium sources against cadmium-induced nephrotoxicity via regulating the transcriptions of selenoproteome. Ecotoxicol Environ Saf 215:112135.

Huang, Y. Q., Y. X. Tang, B. H. Qiu, M. Talukder, X. N. Li, and J. L. Li. 2022. Di-2-ethylhexyl phthalate (DEHP) induced lipid metabolism disorder in liver via activating the LXR/SREBP-1c/ PPARα/γ and NF-κB signaling pathway. Food Chem. Toxicol. 165:113119.

Jamshed, H., R. A. Beyl, D. L. Della Manna, E. S. Yang, E. Ravussin, and C. M. Peterson. 2019. Early time-restricted feeding improves 24-hour glucose levels and affects markers of the circadian clock, aging, and autophagy in humans. Nutrients. 11:1234.

Jiang, J., C. Wu, H. Gao, J. Song, and H. Li. 2010. Effects of astragalus polysaccharides on immunologic function of erythrocyte in chickens infected with infectious bursa disease virus. Vaccine. 28:5614–5616.

Jiang, F. W., Z. Y. Yang, Y. F. Bian, J. G. Cui, H. Zhang, Y. Zhao, and J. L. Li. 2021. The novel role of the aquaporin water channel in lycopene preventing DEHP-induced renal ionic homeostasis disturbance in mice. Ecotoxicol. Environ. Saf. 226:112836.

Jin, M., K. Zhao, Q. Huang, and P. Shang. 2014. Structural features and biological activities of the polysaccharides from Astragalus membranaceus. Int. J. Biol. Macromol. 64:257–266.

Kim, J. H., S. J. Park, T. S. Kim, H. J. Park, J. Park, B. K. Kim, G. R. Kim, J. M. Kim, S. M. Huang, J. I. Chae, C. K. Park, and D. S. Lee. 2013. Testicular hyperthermia induces unfolded protein response signaling activation in spermatocyte. Biochem. Biophys. Res. Commun. 434:861–866.

Li, F., A. M. Shah, Z. Wang, Q. Peng, R. Hu, H. Zou, C. Tan, X. Zhang, Y. Liao, Y. Wang, X. Wang, L. Zeng, B. Xue, and L. Wang. 2019. Effects of land transport stress on variations in ruminal microbe diversity and immune functions in different breeds of cattle. Animals. 9:599.

Li, J., M. A. Ullah, H. Jin, Y. Liang, L. Lin, J. Wang, X. Peng, H. Liao, Y. Li, Y. Ge, and L. Li. 2021. ORMDL3 functions as a negative regulator of antigen-mediated mast cell activation via an ATF6-UPR-autophagy-dependent pathway. Front. Immunol. 12:604974.

Li, Z. Y., J. Lin, F. Sun, H. Li, J. Xia, X. N. Li, J. Ge, C. Zhang, and J. L. Li. 2017. Transport stress induces weight loss and heart injury in chicks: disruption of ionic homeostasis via modulating ion transporting ATPases. Oncotarget. 8:24142–24153.

Li, M. Z., Y. Zhao, H. R. Wang, M. Talukder, and J. L. Li. 2021. Lycopene preventing DEHP-induced renal cell damage is targeted by aryl hydrocarbon receptor. J. Agric. Food Chem. 69:12853–12861.

Lin, J., J. Xia, H. S. Zhao, R. Hou, M. Talukder, L. Yu, J. Y. Guo, and J. L. Li. 2018. Lycopene triggers Nrf2-AMPK cross talk to alleviate atrazine-induced nephrotoxicity in mice. J. Agric. Food Chem. 66:12385–12394.

Liu, L., J. Shen, C. Zhao, X. Wang, J. Yao, Y. Gong, and X. Yang. 2015. Dietary Astragalus polysaccharide alleviated immunological stress in broilers exposed to lipopolysaccharide. Int. J. Biol. Macromol. 72:624–632.

Luo, T., J. Qin, M. Liu, J. Luo, F. Ding, M. Wang, and L. Zheng. 2015. Astragalus polysaccharide attenuates lipopolysaccharide-induced inflammatory responses in microglial cells: regulation of protein kinase B and nuclear factor-kappaB signaling. Inflamm. Res. 64:205–212.

Lystad, A. H., S. R. Carlsson, and A. Simonsen. 2019. Toward the function of mammalian ATG12-ATG5-ATG16L1 complex in autophagy and related processes. Autophagy. 15:1485–1486.

Machovcova, Z., V. Vecerek, E. Voslarova, M. Malena, F. Conte, I. Bedanova, and L. Vecerkova. 2017. Pre-slaughter mortality among turkeys related to their transport. Anim Sci J. 88:705–711.

Oakes, S. A., and F. R. Papa. 2015. The role of endoplasmic reticulum stress in human pathology. Annu. Rev. Pathol. 10:173–194.

Oghbaei, H., L. Hosseini, F. Farajdokht, S. Rahigh Aghsan, A. Majdi, S. Sadigh-Eteghad, S. Sandoghchian Shotorbani, and J. Mahmoudi. 2021. Heat stress aggravates oxidative stress, apoptosis, and endoplasmic reticulum stress in the cerebellum of male C57 mice. Mol. Biol. Rep. 48:5881–5887.

Park, A. M., and Y. J. Suzuki. 2007. Effects of intermittent hypoxia on oxidative stress-induced myocardial damage in mice. J. Appl. Physiol. 102:1806–1814.

Parzych, K. R., and D. J. Klionsky. 2014. An overview of autophagy: morphology, mechanism, and regulation. Antioxid. Redox. Signal. 20:460–473.

Pincus, D., M. W. Chevalier, T. Aragon, E. van Anken, S. E. Vidal, H. El-Samad, and P. Walter. 2010. BiP binding to the ER-stress sensor Ire1 tunes the homeostatic behavior of the unfolded protein response. PLoS Biol. 8:e1000415.

Pittig, A., J. J. Arch, C. W. Lam, and M. G. Craske. 2013. Heart rate and heart rate variability in panic, social anxiety, obsessive-compulsive, and generalized anxiety disorders at baseline and in response to relaxation and hyperventilation. Int. J. Psychophysiol. 87:19–27.

Qi, Z., and L. Chen. 2019. Endoplasmic reticulum stress and autophagy. Adv. Exp. Med. Biol. 1206:167–177.

Qin, D. Z., H. Cai, C. He, D. H. Yang, J. Sun, W. L. He, B. L. Li, J. L. Hua, and S. Peng. 2021. Melatonin relieves heat-induced spermatocyte apoptosis in mouse testes by inhibition of ATF6 and PERK signaling pathways. Zool. Res. 42:514–524.

Santurtun, E., and C. J. Phillips. 2015. The impact of vehicle motion during transport on animal welfare. Res. Vet. Sci. 100:303–308.

Sun, F., Y. Z. Zuo, J. Ge, J. Xia, X. N. Li, J. Lin, C. Zhang, H. L. Xu, and J. L. Li. 2018. Transport stress induces heart damage in newly hatched chicks via blocking the cytoprotective heat shock response and augmenting nitric oxide production. Poult. Sci. 97:2638–2646.

Talukder, M., S. S. Bi, H. T. Jin, J. Ge, C. Zhang, M. W. Lv, and J. L. Li. 2021. Cadmium induced cerebral toxicity via modulating MTF1-MTs regulatory axis. Environ. Pollut. 285:117083.

Vanhoutte, D., T. G. Schips, A. Vo, K. M. Grimes, T. A. Baldwin, M. J. Brody, F. Accornero, M. A. Sargent, and J. D. Molkentin. 2021. Thbs1 induces lethal cardiac atrophy through PERK-ATF4 regulated autophagy. Nat. Commun. 12:3928.

Vegliante, R., and M. R. Ciriolo. 2018. Autophagy and autophagic cell death: uncovering new mechanisms whereby dehydroepiandrosterone promotes beneficial effects on human health. Vitam. Horm. 108:273–307.

Viollet, B., S. Horman, J. Leclerc, L. Lantier, M. Foretz, M. Billaud, S. Giri, and F. Andreelli. 2010. AMPK inhibition in health and disease. Crit. Rev. Biochem. Mol. Biol. 45:276–295.

Wan, C., Y. Chen, P. Yin, D. Han, X. Xu, S. He, M. Liu, X. Hou, F. Liu, and J. Xu. 2016. Transport stress induces apoptosis in rat myocardial tissue via activation of the mitogen-activated protein kinase signaling pathways. Heart Vessels. 31:212–221.

Yin, B., L. Di, S. Tang, and E. Bao. 2020. Vitamin CNa enhances the antioxidant ability of chicken myocardium cells and induces heat shock proteins to relieve heat stress injury. Res. Vet. Sci. 133:124–130.

Yin, H., Z. Zuo, Z. Yang, H. Guo, J. Fang, H. Cui, P. Ouyang, X. Chen, J. Chen, Y. Geng, Z. Chen, C. Huang, and Y. Zhu. 2021. Nickel induces autophagy via PI3K/AKT/mTOR and AMPK pathways in mouse kidney. Ecotoxicol. Environ. Saf. 223:112583.

Zeng, H., Y. Xi, Y. Li, Z. Wang, L. Zhang, and Z. Han. 2020. Analysis of Astragalus polysaccharide intervention in heat-stressed dairy cows' serum metabolomics. Animals. 10:574.

Zhang, C., Z. Y. Geng, K. K. Chen, X. H. Zhao, and C. Wang. 2019. L-theanine attenuates transport stress-induced impairment of meat quality of broilers through improving muscle antioxidant status. Poult. Sci. 98:4648–4655.

Zhao, Y., R. K. Bao, S. Y. Zhu, M. Talukder, J. G. Cui, H. Zhang, X. N. Li, and J. L. Li. 2021a. Lycopene prevents DEHP-induced hepatic oxidative stress damage by crosstalk between AHR-Nrf2 pathway. Environ. Pollut. 285:117080.

Zhao, Y., L. G. Cui, M. Talukder, J. G. Cui, H. Zhang, and J. L. Li. 2021c. Lycopene prevents DEHP-induced testicular endoplasmic reticulum stress via regulating nuclear xenobiotic receptors and unfolded protein response in mice. Food Funct. 12:12256–12264.

Zhao, Y., J. G. Cui, H. Zhang, X. N. Li, M. Z. Li, M. Talukder, and J. L. Li. 2021b. Role of mitochondra-endoplasmic reticulum

coupling in lycopene preventing DEHP-induced hepatotoxicity. Food Funct. 12:10741–10749.

Zhao, Y., Z. H. Du, M. Talukder, J. Lin, X. N. Li, C. Zhang, and J. L. Li. 2018. Crosstalk between unfolded protein response and Nrf2-mediated antioxidant defense in Di-(2-ethylhexyl) phthalate-induced renal injury in quail (*Coturnix japonic*a). Environ. Pollut. 242:1871–1879.

Zhao, Y., H. X. Li, Y. Luo, J. G. Cui, M. Talukder, and J. L. Li. 2022. Lycopene mitigates DEHP-induced hepatic mitochondrial quality control disorder via regulating SIRT1/PINK1/mitophagy axis and mitochondrial unfolded protein response. Environ. Pollut. 292:118390.

Zhao, Y. X., Y. X. Tang, X. H. Sun, S. Y. Zhu, X. Y. Dai, X. N. Li, and J. L. Li. 2022. Gap junction protein connexin 43 as a target is internalized in astrocyte neurotoxicity caused by Di-(2-ethylhexyl) phthalate. J. Agric. Food Chem. 70:5921–5931.

Zhou, R., H. Chen, J. Chen, X. Chen, Y. Wen, and L. Xu. 2018. Extract from Astragalus membranaceus inhibit breast cancer cells proliferation via PI3K/AKT/mTOR signaling pathway. BMC Complement. Altern. Med. 18:83.

Zhu, L., E. Bao, R. Zhao, and J. Hartung. 2009. Expression of heat shock protein 60 in the tissues of transported piglets. Cell Stress Chaperones. 14:61–69.

Zhu, S. Y., J. Y. Guo, J. Y. Li, X. Y. Dai, X. N. Li, and J. L. Li. 2022. Lycopene ameliorates atrazine-induced pyroptosis in spleen by suppressing the Ox-mtDNA/Nlrp3 inflammasome pathway. Food Funct. 13:3551–3560.

Zhu, S. Y., L. L. Liu, Y. Q. Huang, X. W. Li, M. Talukder, X. Y. Dai, Y. H. Li, and J. L. Li. 2021. In silico analysis of selenoprotein N (Gallus gallus): absence of EF-hand motif and the role of CUGS-helix domain in antioxidant protection. Metallomics 13:mfab004.